Extracting Effective Diffusion Parameters from Drying Experiments

Peter E. Price, Jr., Sharon Wang, and Ilyess Hadj Romdhane
3M Engineering Systems and Technology, St. Paul, MN 55144

Thin polymer coatings produced from water- and organic-solvent-based precursor liquids are ubiquitous components of industrial and consumer products. Design and optimization of dryers for these coatings require accurate predictions of their drying rates. Accurate drying predictions for many polymer/solvent coatings require a satisfactory description of the polymer/solvent mutual diffusion coefficients. A method is proposed to determine a satisfactory description of the diffusion coefficients by effective free-volume theory parameters. The effective parameters are determined from gravimetric data measured in a bench-scale drying apparatus. The application of the method to a poly(vinyl acetate)/toluene solution shows that the effective free-volume parameters give diffusion coefficients that agree with published data. The method is also applied to a rubber-based adhesive in industrial-grade heptane by treating the complex adhesive as a pseudobinary solution. For both systems, the effective parameters lead to quantitatively accurate drying predictions in a pilot-scale oven.

Introduction

Industry produces thousands of miles of coated webs each year. Examples include adhesive tapes, photographic films, and magnetic media. The coatings are produced by metering precursor liquids onto moving webs. The coated liquids frequently contain water or organic solvent(s) and polymer(s), and sometimes contain insoluble components, including pigments and magnetic particles. To form the final product, the water or organic solvent(s) must be dried from the coating.

Drying ovens for coated webs can have a variety of configurations, from gentle parallel air flow to vigorous air impingement. Drying is often the last process that can induce fundamental changes in the properties of the coating. Oven conditions may dictate whether the final result is salable material or scrap. Drying ovens also require significant capital investment, so proper design is crucial. There is a strong incentive for developing methods to make quantitatively accurate drying predictions for process design and optimization.

A variety of models for drying thin coatings in convection ovens have appeared in the literature (Robinson et al., 1969; Tu and Drake, 1990; Vrentas and Vrentas, 1994; Gutoff, 1994; Cairncross, 1994, and references therein). The published works offer varying degrees of sophistication. However, there appear to be some minimum general requirements for making accurate predictions of drying in convection ovens: the model must describe the nonisothermal nature of the process, the nonlinear dependence of the polymer/solvent mutual diffusion coefficients on temperature and concentration, and the film shrinkage. We use a model that follows several recently published works (Cairncross et al., 1992; Vrentas and Vrentas, 1994).

For all but very thin coatings with low initial polymer concentrations, the most critical requirement for quantitative drying predictions is an accurate characterization of the falling-rate period of drying. The falling-rate period is generally considered to be the region of diffusion-limited behavior. An accurate characterization of the falling-rate regime requires detailed knowledge of the polymer/solvent mutual diffusion coefficients as functions of concentration and temperature. Diffusion coefficients can be determined from sorption/desorption experiments, NMR or infrared spectroscopic techniques, inverse gas chromatography, and so forth. If experimental data are not available, predictive theories (Zielinski and Duda, 1992) can be used, although they may not lead to quantitatively accurate drying predictions.

Diffusion measurements require considerable time and effort to cover the range of conditions that exist in a drying oven. Furthermore, the established experimental techniques

Correspondence concerning this article should be addressed to P. E. Price, Jr.

are difficult to implement for typical industrial coating solutions that may contain numerous nonvolatile components and may be formulated in industrial-grade solvents containing 15% or more of impurities.

In this article, we propose a technique for determining *effective* parameters for the free-volume theory of diffusion in polymer/solvent systems from a drying model and bench-scale drying experiments. The effective parameters capture the solvent concentration and temperature dependencies of the diffusion coefficients and could conceivably be applied in any application that requires these diffusion coefficients. We apply the technique to poly(vinyl acetate)/toluene solutions and to a complex natural rubber-based industrial adhesive coating. The effective parameters allow us to make quantitative drying predictions for pilot-scale drying of both coatings. We believe that our approach will have considerable value to practicing engineers who seek to apply mathematical models to their drying operations, and more generally to others looking for faster ways to characterize diffusion coefficients in polymer/solvent systems.

Drying Model

Drying involves simultaneous mass, energy, and momentum transport. Vrentas and Vrentas (1994) derived in detail a one-dimensional drying model. We use a similar model and have tried to follow their notation.

Consider a thin slice of a coating on an impermeable substrate (web), as shown in Figure 1. In this article, we assume that the coating may contain multiple nonvolatile components in a single industrial-grade (or better) solvent. We treat such coatings as pseudobinary systems, lumping the components into a single nonvolatile "polymer" and single volatile "solvent." The drying rate at any time depends on how the solvent concentration and temperature profiles develop as the coating moves through the drying oven. To compute the concentration and temperature profiles, we follow the assumptions of Vrentas and Vrentas (1994), except that we allow for conductive transport in the web and coating and radiant energy fluxes to the surfaces of the substrate and coating.

The solvent mass balance in the polymer (coating) phase is

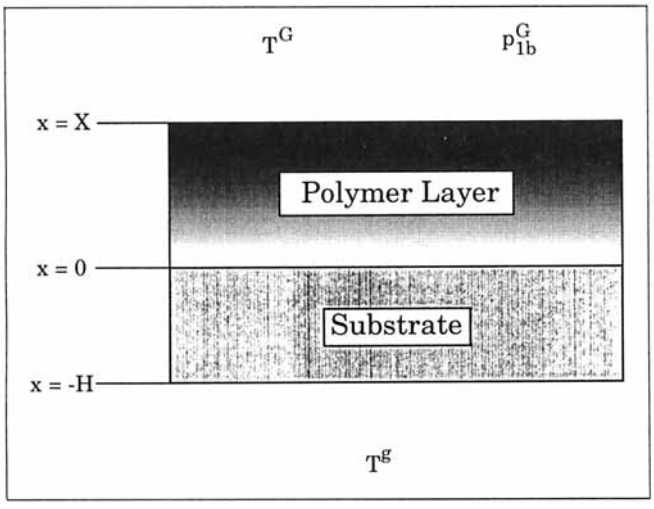

Figure 1. Model system.

$$\frac{\partial \rho_1^P}{\partial t} = \frac{\partial}{\partial x}\left(D^P \frac{\partial \rho_1^P}{\partial x} \right) \tag{1}$$

where $\rho_1^P(x,t)$ is the solvent concentration in the polymer phase; t is time; x is the position in the direction normal to the coating/substrate interface within the polymer phase; $D^P(\rho_1^P, T^P)$ is the polymer/solvent mutual diffusion coefficient.

The concentration and temperature dependencies of the mutual diffusion coefficients, D^P, are described by free-volume theory (Vrentas and Duda, 1977a,b):

$$D^P = QD_0 \exp\left[\frac{-E}{RT^P}\right] \exp\left[\frac{-\gamma\left(\omega_1^P \hat{V}_1^* + \omega_2^P \xi \hat{V}_2^*\right)}{\hat{V}_{FH}}\right], \tag{2}$$

where

$$Q = (1-\phi_1^P)^2(1-2\chi\phi_1^P) \tag{3}$$

and

$$\frac{\hat{V}_{FH}}{\gamma} = \frac{K_{11}}{\gamma}\omega_1^P\left(K_{21}+T^P-T_{g1}\right) + \frac{K_{12}}{\gamma}\omega_2^P\left(K_{22}+T^P-T_{g2}\right), \tag{4}$$

where D_0 is the preexponential factor; E is the activation energy, R is the gas constant; K_{11}/γ and $K_{21}-T_{g1}$ are free-volume parameters for the solvent; K_{12}/γ and $K_{22}-T_{g2}$ are free-volume parameters for the polymer; $\hat{V}_1^*$ and $\hat{V}_2^*$ are the solvent- and polymer-specific critical hole free-volumes; ξ is the ratio of the solvent and polymer critical molar jumping unit volumes; and χ is the Flory–Huggins parameter.

The coating solution is assumed to be ideal. In an ideal solution there is no volume change in mixing. The polymer phase mass fractions, ω_i^P, and volume fractions, ϕ_i^P, are then related to the local solvent and polymer densities by the equations

$$\omega_1^P = \frac{\rho_1^P}{\rho_1^P + \rho_2^P} \qquad \omega_2^P = 1-\omega_1^P \tag{5}$$

$$\phi_1^P = \rho_1^P \hat{V}_1 \qquad \phi_2^P = \rho_2^P \hat{V}_2 = 1-\phi_1^P, \tag{6}$$

where $\hat{V}_1$ and $\hat{V}_2$ are solvent- and polymer-specific volumes.

There is no flux of solvent through the web:

$$\frac{\partial \rho_1^P}{\partial x} = 0 \qquad \text{at} \quad x = 0. \tag{7}$$

A mass-transfer coefficient, k_1^G, determines the solvent flux from the coating surface:

$$D^P \frac{\partial \rho_1^P}{\partial x} + \rho_1^P \frac{dX}{dt} = -k_1^G\left[p_{1i}^G - p_{1b}^G\right] \qquad \text{at} \quad x = X, \tag{8}$$

where p_{1i}^G is the equilibrium solvent partial pressure at the

coating/air interface, and p_{1b}^G is the solvent partial pressure in the bulk air.

The initial solvent concentration is uniform:

$$\rho_1^P(x,0) = \rho_{10}^P. \tag{9}$$

We assume local equilibrium at the coating surface, and use the Flory–Huggins theory to describe the solvent partial pressure:

$$p_{1i}^G = P_1 \phi_1^P \exp\left[\phi_2^P + \chi(\phi_2^P)^2\right]. \tag{10}$$

The Antoine equation describes the pure solvent vapor pressure as a function of temperature:

$$\log P_1 = A - \frac{B}{T^P(X,t) + C}, \tag{11}$$

where A, B, and C are Antoine coefficients.

A volume conservation equation takes the place of the total mass balance:

$$\frac{dX}{dt} = -k_1^G \hat{V}_1 [p_{1i}^G - p_{1b}^G]. \tag{12}$$

The initial condition for the position of the coating surface is $X(0) = L$.

The energy balance for the substrate is

$$\rho^S c_p^S \frac{\partial T^S}{\partial t} = \kappa^S \frac{\partial^2 T^S}{\partial x^2}, \tag{13}$$

where ρ^S, c_p^S, and κ^S are the constant substrate density, specific heat, and thermal conductivity, respectively.

A heat-transfer coefficient, h^g, characterizes the convective/conductive energy transfer from the oven air to the lower substrate surface. We assume the oven and web can be treated, to a first approximation, as infinite parallel gray plates and use the Stefan–Boltzmann law to describe the radiant energy flux to the substrate:

$$\kappa^S \frac{\partial T^S}{\partial x} = h^g [T^S - T^g] + \frac{\sigma}{\frac{1}{\epsilon^S} + \frac{1}{\epsilon^l} - 1} [T^{S^4} - T^{l^4}] \quad \text{at} \quad x = -H, \tag{14}$$

where ϵ^S and ϵ^l are the emissivity of the substrate and lower oven wall, respectively; σ is the Stefan–Boltzmann constant; and T^l is the temperature of the lower oven wall. In most cases, it will be equal to T^g, the bulk air temperature below the web.

Here we have assumed that the radiant energy flux is absorbed at the surface of the backing. A more rigorous treatment would include the radiant energy flux as a body-heating term, perhaps using the Lambert–Beer law as did Cairncross et al. (1995). A complete application of the body-heating term, however, would require a detailed understanding of the infrared emission spectrum of the oven surfaces as well as the wavelength dependence of the substrate absorption coefficient. Such an approach is beyond the scope of this article.

The energy balance for the coating is

$$\rho^P c_P^P \frac{\partial T^P}{\partial t} = \frac{\partial}{\partial x}\left(\kappa^P \frac{\partial T^P}{\partial x}\right) + D^P \left(c_{p,1} - \frac{\hat{V}_1}{\hat{V}_2} c_{p,2}\right) \frac{\partial \rho_1^P}{\partial x} \frac{\partial T^P}{\partial x}, \tag{15}$$

where we use time-dependent mass average values for ρ^P, c_p^P, and κ^P based on constant values for the solvent and polymer. The second term on the righthand side describes the flux of energy associated with diffusion of the solvent and polymer in the coating. Test calculations, described in the Appendix, indicate that this term can be neglected for the present calculations. We have done so below.

The temperature and energy flux are constant across the coating/web interface:

$$T^S(0^-,t) = T^P(0^+,t) \tag{16}$$

$$\kappa^S \frac{\partial T^S}{\partial x}(0^-,t) = \kappa^P \frac{\partial T^P}{\partial x}(0^+,t). \tag{17}$$

At the upper surface of the coating, a heat-transfer coefficient, h^G, characterizes the convective/conductive energy transport from the surrounding air. To characterize the radiant energy flux to the surface of the coating, we again treat the web and oven as infinite parallel gray plates. Energy is also carried from the top surface with the evaporating solvent:

$$-\kappa^P \frac{\partial T^P}{\partial x} = h^G [T^P - T^G] + \frac{\sigma}{\frac{1}{\epsilon^P} + \frac{1}{\epsilon^u} - 1} [T^{P^4} - T^{u^4}] + \Delta \hat{H}_{\text{vap},1} k_1^G [p_{1i}^G - p_{1b}^G] \quad \text{at} \quad x = X, \tag{18}$$

where $\Delta \hat{H}_{\text{vap},1}$ is the heat of vaporization of the solvent; ϵ^P and ϵ^u are the coating and upper oven wall emissivities, respectively; T^u is the temperature of the upper oven wall. Typically, T^u will equal T^G, the bulk air temperature above the coating.

As discussed earlier, one could include the radiant energy flux from the upper oven surfaces as a body-heating term in the energy balance using, for example, the Lambert–Beer law. A rigorous application of this approach would be even more complicated for the coating than for the backing, since the absorption coefficient in the coating will vary with composition as well as wavelength.

The initial temperature in the polymer and substrate phases is uniform:

$$T^P(x,0) = T^S(x,0) = T_0. \tag{19}$$

The heat- and mass-transfer coefficients are related by a Chilton–Coburn analogy (Kreith, 1973):

$$\frac{h^G M_1}{k_1^G} = \rho_{\text{air}} c_{p,\text{air}} R\bar{T} \left[\frac{\rho_{\text{air}} c_{p,\text{air}} D_{1,\text{air}}}{\kappa_{\text{air}}}\right]^{-0.67}, \tag{20}$$

where M_1 is the solvent molecular weight; ρ_{air}, $c_{p,air}$, and κ_{air} are the density, specific heat, and thermal conductivity of the air evaluated at the average temperature, $\bar{T} = [T^P(X) + T^G]/2$; and $D_{1,air}$ is the diffusivity of the solvent in air at the average temperature $\bar{T}$.

Typically, the heat-transfer coefficients in a drying oven are computed from correlations generated by manufacturing engineers or by drying-oven vendors. These correlations relate the heat-transfer coefficient to such things as the air velocity and nozzle spacing. The preceding correlation is then used to compute a corresponding mass-transfer coefficient. Equation 20 only relates the heat- and mass-transfer coefficients when the former does not include a significant contribution from radiative energy transport.

We put the model in dimensionless form by defining:

$$T^{S*} = \frac{T^S}{T_0} \qquad T^{P*} = \frac{T^P}{T_0} \qquad c = \frac{\rho_1^P}{\rho_{10}^P}$$

$$t^* = \frac{D_0^P t}{L^2} \qquad \eta = \frac{x}{X(t)} \qquad \zeta = \frac{x}{H}$$

$$X^* = \frac{X}{L} \qquad T^{g*} = \frac{T^g}{T_0} \qquad T^{G*} = \frac{T^G}{T_0}.$$

$$T^{l*} = \frac{T^l}{T_0} \qquad T^{u*} = \frac{T^u}{T_0} \tag{21}$$

The dimensionless equations are

$$X^* \frac{\partial c}{\partial t^*} = \frac{1}{X^*} \frac{\partial}{\partial \eta}\left(\frac{D^P}{D_0^P} \frac{\partial c}{\partial \eta} \right) + \eta \frac{dX^*}{dt^*} \frac{\partial c}{\partial \eta} \tag{22}$$

$$\frac{\partial c}{\partial \eta} = 0 \qquad \text{at} \quad \eta = 0 \tag{23}$$

$$\frac{1}{X^*} \frac{D^P}{D_0^P} \frac{\partial c}{\partial \eta} + c \frac{dX^*}{dt^*} = -\frac{k_1^G L P_{tot}}{D_0^P \rho_{10}^P} [y_{1i}^G - y_{1b}^G] \qquad \text{at} \quad \eta = 1 \tag{24}$$

$$c(\eta, 0) = 1 \tag{25}$$

$$\frac{dX^*}{dt^*} = -\frac{k_1^G \hat{V}_1^P L P_{tot}}{D_0^P} [y_{1i}^G - y_{1b}^G] \tag{26}$$

$$X^*(0) = 1 \tag{27}$$

$$\frac{\partial T^{S*}}{\partial t^*} = \frac{\kappa^S L^2}{\rho^S c_p^S H^2 D_0^P} \frac{\partial^2 T^{S*}}{\partial \zeta^2} \tag{28}$$

$$\frac{\partial T^{S*}}{\partial \zeta} = \frac{h^g H}{\kappa^S} [T^{S*} - T^{g*}] + \frac{\sigma T_0^3 H}{\kappa^S \left(\frac{1}{\epsilon^S} + \frac{1}{\epsilon^l} - 1 \right)} [T^{*4} - T^{l*4}]$$

$$\text{at} \quad \zeta = -1 \tag{29}$$

$$T^{S*}(0^-, t^*) = T^{P*}(0^+, t^*) \tag{30}$$

$$\frac{\partial T^{S*}}{\partial \zeta}(0^-, t^*) = \frac{\kappa^P H}{\kappa^S L} \frac{1}{X^*} \frac{\partial T^{P*}}{\partial \eta}(0^+, t^*) \tag{31}$$

$$X^* \frac{\rho^P c_p^P}{\rho^{ref} c_p^{ref}} \frac{\partial T^{P*}}{\partial t^*} = \frac{1}{X^*} \frac{\partial}{\partial \eta}\left(\frac{\kappa^P}{\rho^{ref} c_p^{ref} D_0^P} \frac{\partial T^{P*}}{\partial \eta} \right) + \eta \frac{dX^*}{dt^*} \frac{\rho^P c_p^P}{\rho^{ref} c_p^{ref}} \frac{\partial T^{P*}}{\partial \eta} \tag{32}$$

$$-\frac{1}{X^*} \frac{\partial T^{P*}}{\partial \eta} = \frac{h^G L}{\kappa^P} [T^{P*} - T^{G*}] + \frac{\sigma T_0^3 L}{\kappa^P \left(\frac{1}{\epsilon^P} + \frac{1}{\epsilon^u} - 1 \right)} \times [T^{P*4} - T^{u*4}] + \frac{\Delta H_{vap,1} k_1^G L P_{tot}}{\kappa^P T_0} [y_{1i}^G - y_{1b}^G] \qquad \text{at} \quad \eta = 1 \tag{33}$$

$$T^{P*}(\eta, 0) = T^{S*}(\zeta, 0) = 1, \tag{34}$$

where ρ^{ref} and c_p^{ref} are the reference density and specific heat used to scale the energy-transport equation in the polymer phase; P_{tot} is the total pressure in the oven; y_{1i}^G is the solvent mole fraction at the coating/air interface; and y_{1b}^G is the solvent mole fraction in the bulk air above the coating.

Numerical Methods

The mass and energy balances were discretized using Galerkin's method with finite-element basis functions. In this approach, the solvent concentration and temperature profiles are approximated as series of weighted piecewise-linear basis functions ψ_i:

$$T^{S*} = \sum_{i=1}^{N_S} u_i(t^*) \psi_i(\zeta) \qquad T^{P*} = \sum_{j=1}^{N_P} u_{N_S+2j-1}(t^*) \psi_j(\eta)$$

$$c = \sum_{j=1}^{N_P} u_{N_S+2j}(t^*) \psi_j(\eta) \qquad X^* = u_{N_S+2N_P+1}. \tag{35}$$

The first N_S elements of the solution vector, $\boldsymbol{u}$, contain the temperature coefficients of the substrate series. The next $2N_p$ elements of $\boldsymbol{u}$ contain alternating coefficients of the polymer phase temperature and solvent concentration. The final element of $\boldsymbol{u}$ is the film height.

In Galerkin's method, the residuals are set orthogonal to the basis functions (Dhatt and Touzot, 1984). This leads to a set of ordinary differential equations:

$$\boldsymbol{g}(\boldsymbol{u}, t^*) = \boldsymbol{M} \frac{d\boldsymbol{u}}{dt} - \boldsymbol{r}(\boldsymbol{u}) = \boldsymbol{0}. \tag{36}$$

We integrated this system of ordinary differential equations using DASSL (Petzold, 1983) with the integrator error tolerances set to 10^{-6}.

Extracting Diffusion Parameters from Drying Data

The typical approach to drying predictions is first to measure diffusion coefficients by one of the accepted techniques; then to regress free-volume theory parameters from these measurements; and finally to use the parameters to make

drying predictions to compare with experimental data. When this work began, our hypothesis was that we could treat the inverse problem of characterizing the polymer/solvent mutual diffusion coefficients from gravimetric drying data. We sought to determine *effective* free-volume theory parameters for Eqs. 2 through 4 that would yield predictions to match measured drying curves. To test this hypothesis, we needed to obtain detailed drying data, to develop a computer program to regress the effective free-volume theory parameters, and to apply and confirm the method with several polymer/solvent systems.

Bench-scale measurements of detailed drying data

To obtain detailed drying data, we conducted bench-scale drying studies with an Ohaus MB-200 moisture determination balance (Ohaus Corp., Florham Park, NJ). The Ohaus MB-200 consists of a scale (accurate to 0.01 g) inside of a programmable oven. The oven temperatures can be programmed so that the sample is subjected to as many as three temperatures for up to 180 min per temperature. The oven is heated with an infrared heating coil. The temperature in the oven chamber is controlled by means of a thermocouple in the air space just above the sample. Our samples consist of 3 to 5 g of solution in 5-cm-diameter aluminum sample pans. The Ohaus MB-200 oven is designed to allow natural convective air flow to carry away solvent vapor. We have the oven in a laboratory hood that provides additional air flow through the oven chamber. The Ohaus MB-200 sends time, air temperature, and sample weight data every 10 s to a personal computer via an RS-232 interface. When subjected to the same temperature programs, samples of the same initial weight yield virtually identical drying curves, indicating the excellent reproducibility of the apparatus. The apparatus is shown in Figure 2. The apparatus is similar in principle to a thermal gravimetric analyzer (TGA), albeit with less precision. The Ohaus MB-200 does, however, allow much larger sample sizes than a TGA. This alleviates the edge effects that may compromise comparisons between drying models and the small samples in a TGA.

The polymer/solvent samples in our studies were subjected to a three-temperature program that included an initial low-temperature region, and intermediate-temperature region, and a high-temperature final region. Although this three-temperature program was not critical to the results shown here, it is necessary to study the drying behavior at temperatures above the boiling point of the initial solution. If the temperature is raised too quickly, the solution will boil, creating bubbles that destroy the uniform thickness of the sample and render the experimental data useless. An initial low-temperature period will raise the boiling point of the sample by increasing the polymer concentration. The drying behavior at higher temperatures can then be examined without boiling the sample. The final high-temperature region serves to determine the precise amount of nonvolatiles in the sample. We used only the data from the first two temperature periods and the final dry weight in our analysis.

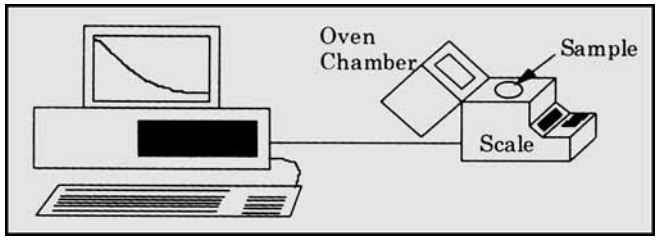

Figure 2. Moisture determination balance apparatus.

Regression of effective free-volume parameters

The free-volume theory expression for the mutual diffusion coefficients in a binary polymer/solvent system, Eqs. 2 through 4, contains nine parameters. To reduce the number of effective parameters to be regressed, we sought estimates of as many of the free-volume theory parameters as possible. We follow Zielinski and Duda (1992) and set the activation energy, E, to zero. The free-volume parameters K_{11}/γ and $K_{21}-T_{g1}$ for many common solvents are available in the literature (Zielinski and Duda, 1992). We have successfully used literature values for pure solvents even in cases where our solvent was industrial-grade. Since Eq. 2 contains only the product $\xi\hat{V}_2^*$, we treat this product as a single parameter. Assuming we can measure or estimate the Flory–Huggins parameter, χ, and the remaining physical properties of the solution, we are left with four diffusion parameters to regress: D_0, $\xi\hat{V}_2^*$, K_{12}/γ, and $K_{22}-T_{g2}$.

The four unknown parameters were regressed from the bench-top drying data by minimizing the sum of the squares of the normalized differences between the experimental and predicted residual solvent values at each time step of the experiments. Normalized differences were computed as follows:

$$\mathrm{FVEC}_i = \left| \frac{\left(\dfrac{\text{Solvent weight at } t_i(g)}{\text{Sample area (cm}^2)}\right)_{\text{exp}} - \left(\int_0^{X(t_i)} \rho_1(x,t_i)\,dx\right)_{\text{model}}}{\left(\dfrac{\text{Solvent weight at } t_i(g)}{\text{Sample area (cm}^2)}\right)_{\text{exp}}} \right| \qquad i=1, \mathrm{N}_{\text{exp}}, \quad (37)$$

where N_{exp} is the total number of experimental data points from all of the experiments used in the regression analysis.

To solve the nonlinear least-squares problem, we used the modified Levenberg–Marquardt code LMDIF1 (Garbow et al., 1980). LMDIF1 requires a subroutine to calculate the N_{exp} functions, FVEC_i, to be minimized. For the present problem, that subroutine contained the finite-element formulation of our drying model. The initial coating weights and heat-transfer conditions used in the model calculations were chosen to correspond to the experimental conditions within the limitations of the model, as discussed below. The subroutine was set up to integrate from one experimental time value to the next for all of the experimental drying curves used in the regression analysis. At each step of the integration, the function just given was computed. The final vector of N_{exp} functions was then returned to LMDIF1.

LMDIF1 does not necessarily return globally optimum free-volume parameters. Our procedure involves starting the regressions from several initial values of the unknown free-volume parameters and choosing the values leading to the

lowest sum-of-squared errors. We have found that there may be multiple sets of parameters that yield similar sum-of-squared errors. Frequently, these different sets of parameters yield similar mutual diffusion coefficients as functions of concentration and temperature in the range of interest. We have also found that there are fewer local optima when the experimental data are based on samples of varying thickness that have been subjected to a range of oven temperatures. Of course, whether or not any set of estimated and regressed parameters are reasonable ultimately depends only upon whether or not they lead to accurate predictions of the drying rate of a coating. Additional support for a given set of parameters may be obtained by comparing predictions with additional bench-top or pilot-scale experiments, as we show below. The ultimate test is the production line. Since we do not seek any physical insight from the regressed parameters, all sets of regressed parameters that lead to similar values of the mutual diffusion coefficients as functions of concentration and temperature, and thus to similar drying predictions, are considered equally useful.

The objective function for regressing effective diffusion parameters, Eq. 37, uses the drying model described earlier to represent the drying conditions of the samples in the Ohaus MB-200. The drying conditions that the experimental samples experience in the Ohaus MB-200 are not typical of the conditions experienced by a coated web in a convection oven. The Ohaus samples are much thicker than a typical coating, are heated only with a radiative source, and are subjected to relatively low external mass-transfer rates. Since the drying model corresponds to a coated web in a convection oven, we make a few additional assumptions in order to apply it in the regression analysis. We assume that the samples are of uniform thickness, dry at a uniform rates per unit area, and rapidly approach the programmed oven temperature. This last assumption is critical and allows us to ignore the complexities of the radiative heating that occurs in the oven. Instead of treating the radiative heating problem, we assume that the substrate (in this case, the sample pan) has a negligible thermal mass and set the backside heat-transfer coefficient to 10^{-1} cal/s·cm^2·°C. This causes the computed sample temperature to rapidly approach the oven setpoint. We then set the topside heat-transfer coefficient, and thus the topside mass-transfer coefficient computed from Eq. 20, so that the initial drying rates for the sample and model are the same.

There is clearly room for improvement in our treatment of the sample temperature in the regression analysis. One approach would be to account explicitly for the radiative heating. Given the geometry of the heater, the changing infrared absorption coefficients in the drying solution, the varying heating coil temperature, and so on, this approach seems prohibitively complex. A more practical approach may be to insulate the scale surface and then modify the apparatus to control the heater, based on a thermocouple imbedded in the solution or from an optical pyrometer aimed at the coating. The actual coating temperature could then be input as a known parameter in the regression analysis. To date, however, we have found our present approach to be adequate for the many coatings we have studied.

Case studies and confirmation

Figure 3 shows the experimental data and the model regression for two bench-top experiments with poly(vinyl acetate) (Aldrich Chemical #18,948-0, Aldrich Chemical, Milwaukee, WI) in toluene (Aldrich Chemical #17,941-8). The complete set of previously determined and regressed model parameters is shown in Table 1. The substrate parameters shown in Table 1 correspond to the pilot oven predictions discussed below. The solvent free-volume parameters K_{11}/γ and $K_{21} - T_{g1}$ and the Flory–Huggins parameter χ are from Duda (1983). The final sum-of-squared errors for the 2,700

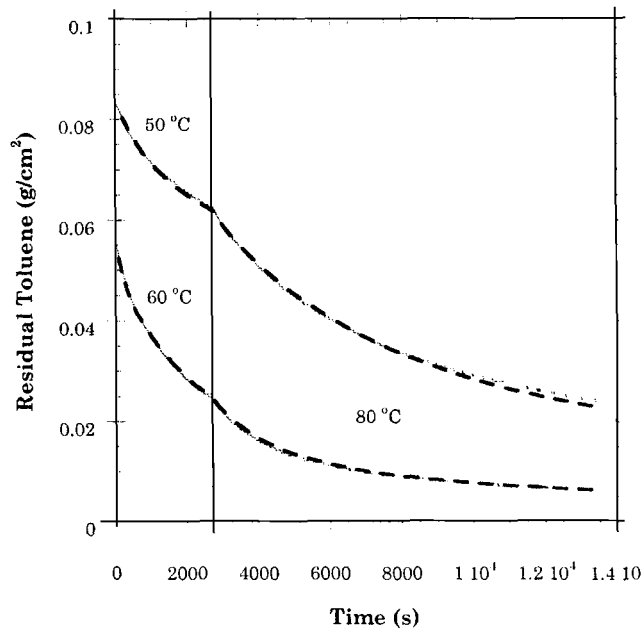

Figure 3. Experimental (solid line) and fitted (dashed line) drying curves for poly(vinyl acetate) in toluene.

Coating-side heat-transfer coefficients are 2.75×10^{-5} cal/s·cm^2·°C for the 60°C/80°C experiment and 2.04×10^{-5} cal/s·cm^2·°C for the 50°C/80°C experiment. Dry-sample weights are 0.05755 g/cm^2 and 0.1024 g/cm^2, respectively.

Table 1. Drying Model Parameters for Poly(vinyl acetate) and Toluene*

Substrate Properties		Polymer Properties	
ρ^S (g/cm^3)	1.38	ρ_2 (g/cm^3)	1.17
$c_{p_S}^S$ (cal/g·K)	0.45	$c_{p,2}$ (cal/g·K)	0.35
κ^S (cal/s·cm·K)	3.22×10^{-4}	κ_2 (cal/s·cm·K)	3.5×10^{-4}
H (cm)	3.556×10^{-3}		
Solvent Properties			
ρ_1 (g/cm^3)	0.866	A	4.07383
$c_{p,1}$ (cal/g·K)	0.44	B	1344.8
κ_1 (cal/s·cm·K)	3.475×10^{-4}	C	−53.668
M_1 (g/mol)	92.14	χ	0.39
$\Delta H_{vap,1}$ (cal/g)	98.89		
Diffusion Parameters			
D_0 (cm^2/s)	**3.998×10^{-4}**	K_{12}/γ (cm^3/g·K)	**6.145×10^{-4}**
E_a (kcal/mol)	0.0	$K_{12} - T_{g2}$ (K)	**−223.9**
ξ	**0.958**	$\hat{V}_1^*$ (cm^3)	0.917
K_{11}/γ (cm^3/g·K)	2.21×10^{-3}	$\hat{V}_2^*$ (cm^3)	1.0
$K_{21} - T_{g1}$ (K)	−103.0		

*Substrate properties correspond to polyester web used in pilot-scale studies. Regressed parameters are in boldface.

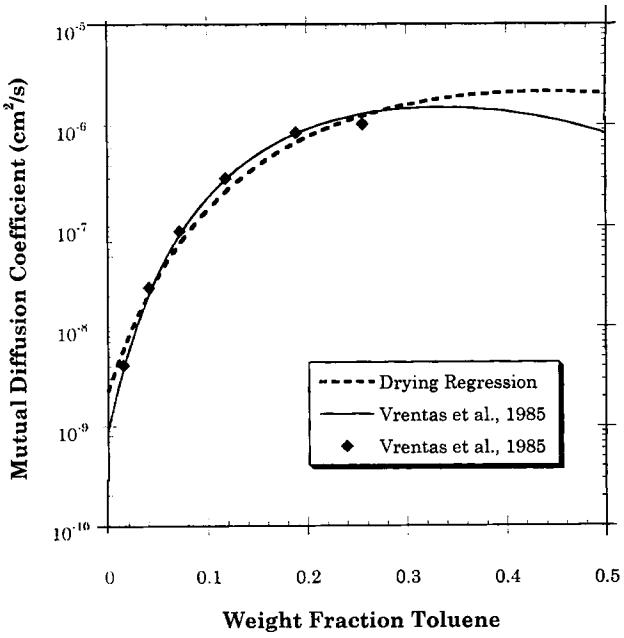

Figure 4. Poly(vinyl acetate)/toluene mutual diffusion coefficients as functions of toluene concentration at 80°C from regressed free-volume parameters in Table 1, experimental data (Vrentas et al., 1985), and a correlation to the data (Vrentas et al., 1985).

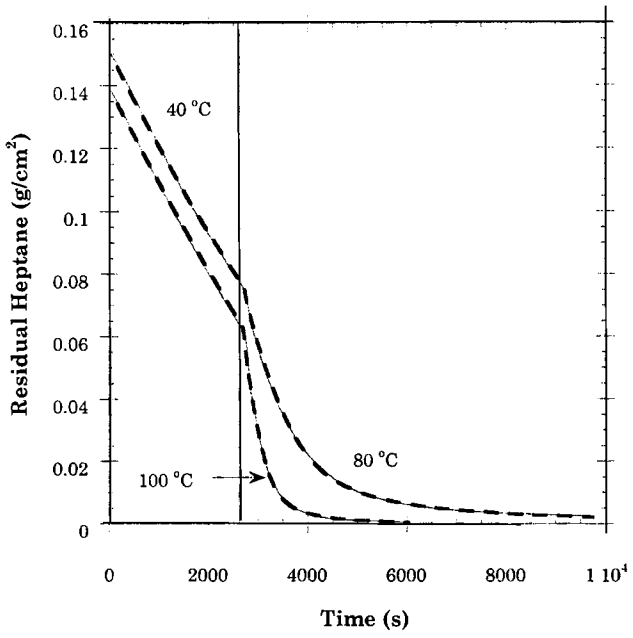

Figure 5. Experimental (solid line) and regressed (dashed line) drying curves for natural rubber-based adhesive in industrial-grade heptane.

Coating-side heat-transfer coefficients are 4.75×10^{-5} cal/s·cm²·°C for the 40°C/80°C experiment and 4.44×10^{-5} cal/s·cm²·°C for the 40°C/100°C experiment. Dry-sample weights are 0.06264 g/cm² and 0.04584 g/cm², respectively.

data points is 1.59. Figure 4 shows the poly(vinyl acetate)/toluene mutual diffusion coefficients as functions of toluene concentration at 80°C based on free-volume parameters and experimental data from the literature (Vrentas et al., 1985), as well as the regressed parameters.

Figure 5 shows the experimental data and the regression results for a more complex, natural rubber-based, industrial adhesive. The adhesive contains several nonvolatile components in industrial-grade heptane. The complete set of previously determined and regressed model parameters is shown in Table 2. The substrate parameters shown in Table 2 correspond to the pilot oven predictions discussed below. We determined the heptane free-volume parameters K_{11}/γ and $K_{21}-T_{g1}$ by interpolation between values for hexane and octane given by Zielinski and Duda (1992). The final sum-of-squared errors for the 517 data points is 0.34. When drying this adhesive, we recorded only the data corresponding to the first occurrence of each decreasing weight valve. Hence, the spacing of the data points varies and is, in general, greater than 10 s. Figure 6 shows the corresponding polymer/solvent mutual diffusion coefficients as functions of heptane concentration at several temperatures.

In cases where no independent diffusion data are available, the regressed parameters can be tested by comparing model predictions with other bench-top experiments. Figure 7 shows such a comparison for an experiment with the rubber-based industrial adhesive at a temperature within the range of the original sample temperatures. The sum-of-squared errors for the 292 data points is 1.335. The agreement suggests that the regressed parameters have captured the diffusion behavior of this system. This assessment is confirmed in our pilot studies, discussed below.

Pilot-Scale Drying Studies

From our industrial perspective, the ultimate goal is to be able to predict residual solvent levels in a coating after it passes through a drying oven. To provide data with which to further test our diffusion characterizations and drying model, we also conducted some pilot-scale drying studies where we measured residual solvent levels for the two coatings. We used an 8-foot-long pilot oven in either a parallel flow or an air floatation configuration. Figure 8 shows the oven. We stud-

Table 2. Drying Model Parameters for Rubber-based Adhesive and Industrial-grade Heptane*

Substrate Properties		Polymer Properties	
ρ_{sub} (g/cm³)	1.38	ρ_2 (g/cm³)	0.7
$c_{p,sub}$ (cal/g·K)	0.45	$c_{p,2}$ (cal/g·K)	0.5
κ_{sub} (cal/s·cm·K)	3.22×10^{-4}	κ_2 (cal/s·cm·K)	4.0×10^{-4}
X_{sub} (cm)	3.556×10^{-3}		
Solvent Properties			
ρ_1 (g/cm³)	0.6837	A	4.02159
$c_{p,1}$ (cal/g·K)	0.54	B	1,268.115
κ_1 (cal/s·cm·K)	3.5×10^{-4}	C	−56.25
M_1 (g/mol)	100.2	χ	0.3
$\Delta H_{vap,1}$ (cal/g)	86.94		
Diffusion Parameters			
D_0 (cm²/s)	$\mathbf{3.446\times10^{-3}}$	K_{12}/γ (cm³/g·K)	$\mathbf{6.145\times10^{-4}}$
E_a (kcal/mol)	0.0	$K_{12}-T_{g2}$ (K)	**−198.6**
ξ	**0.846**	$\hat{V}_1^*$ (cm³)	1.127
K_{11}/γ (cm³/g·K)	1.28×10^{-3}	$\hat{V}_2^*$ (cm³)	1.0
$K_{21}-T_{g1}$ (K)	−32.055		

*Substrate properties correspond to polyester web used in pilot-scale studies. Regressed parameters are in boldface.

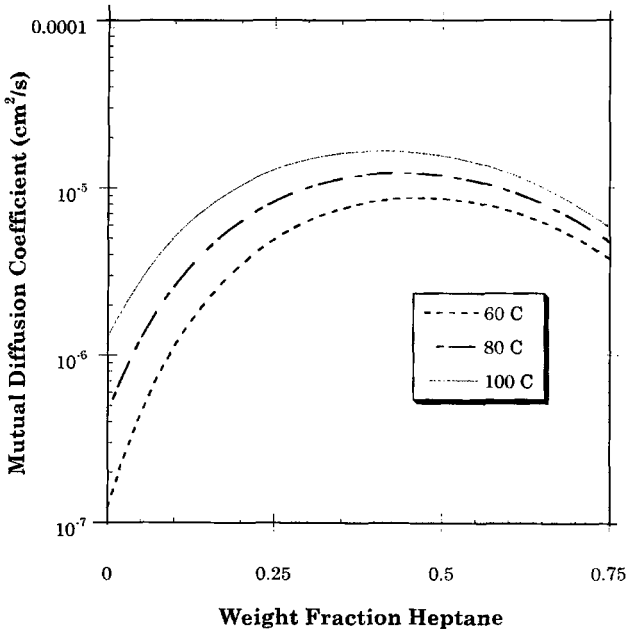

Figure 6. Effective mutual diffusion coefficients for industrial-grade heptane in natural rubber-based adhesive as functions of mass-fraction heptane and temperature.

The diffusion coefficients are based on free-volume parameters regressed from bench-top drying curves, as listed in Table 2.

ied the drying behavior of poly(vinyl acetate)/toluene in the parallel-flow configuration and the rubber-based industrial adhesive in the floatation configuration.

In the parallel-flow drying studies of poly(vinyl acetate)/toluene coatings, we used a beta gauge (LFE Corp., Waltham,

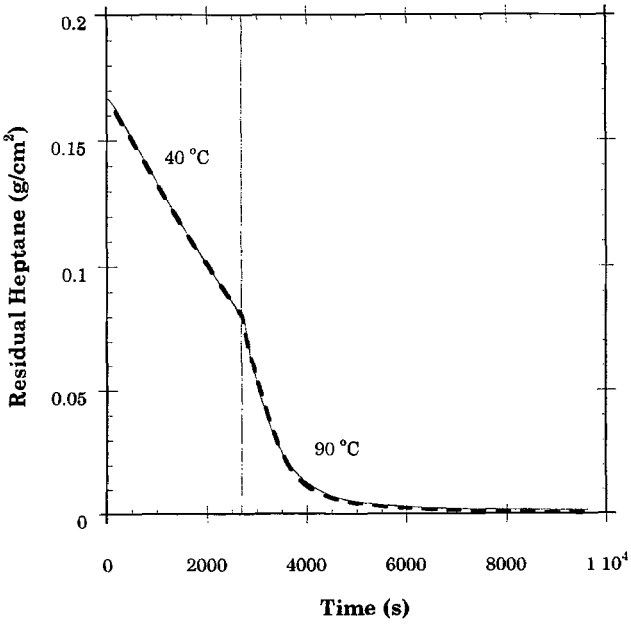

Figure 7. Experimental (solid line) and predicted (dashed line) drying curves for natural rubber-based adhesive in industrial-grade heptane.

The coating-side heat-transfer coefficient is 5.46×10^{-5} cal/s·cm^2·°C. The dry-sample weight is 0.054 g/cm^2.

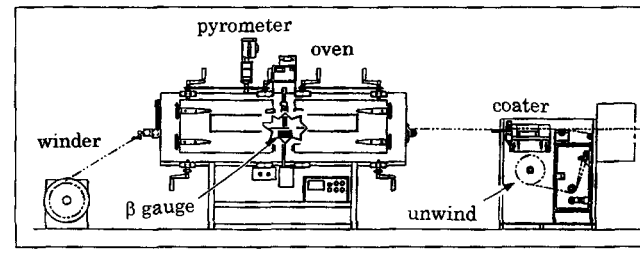

Figure 8. Pilot drying facilities.

MA) and pyrometer to measure the coating mass and temperature vs. time. The beta gauge uses a krypton-85 source and detector to generate a voltage signal that is proportional to the mass of the coating and backing. In these experiments, we coated a section of the web and stopped it in the oven under the beta gauge and pyrometer. The beta gauge and pyrometer data were recorded on a personal computer. The beta gauge data were subsequently scaled to give coating weight vs. time as follows: at the end of the data-collection period, the web was pulled from the oven and a 4 in.$\times$6 in. (102 mm$\times$152 mm) sample from the area that had been under the beta gauge was removed. This sample was weighed, baked in an oven for 30 min at 120°C, and weighed again. We peeled the dry coating from the backing and weighed the backing. From the final mass per unit area of the baked, coated sample and the mass per unit area of the uncoated backing, we determined the polymer coating mass per unit area. We knew the initial mass fraction of polymer in the coating, so this served to determine the initial mass of the coating per unit area. The measured masses per unit area were used to linearly map the beta gauge voltages to values of mass per unit area vs. time. Ultimately, these data were converted to values of residual solvent per unit area vs. time to compare with the drying model predictions.

Figure 9 shows the results of a pilot-scale experiment where we coated 30% solids poly(vinyl acetate) in toluene onto a 3.56×10^{-3}-cm-thick polyester web. The pilot drying oven was set in a parallel-flow configuration at 80°C. The figure also shows predictions of the drying curve based on the parameters listed in Table 1. In the parallel-flow configuration, the oven is fitted with aluminum plates above and below the web. We established the emissivity of these plates by placing them under the pyrometer and adjusting the pyrometer emissivity until the pyrometer temperature matched the known plate/oven air temperature. We determined the heat-transfer coefficients for these calculations by matching the model to measurements on another coating that showed no significant falling-rate period. Thus, the calculations were made without adjusting any of the model parameters.

Figure 10 shows predicted vs. measured residuals for the natural rubber-based industrial adhesive coated onto 3.56×10^{-3}-cm polyester. In these studies, the pilot oven was configured with six air floatation nozzles (Downham et al., 1970) on top and four on the bottom. We coated samples at different web speeds and thicknesses, and measured solvent residuals gravimetrically from samples removed at the oven exit. The predictions are based on the parameters in Table 2. During this set of experiments, we did not gather data on the falling-rate-free solution, so we computed the heat-transfer coefficients for the corresponding calculations using a corre-

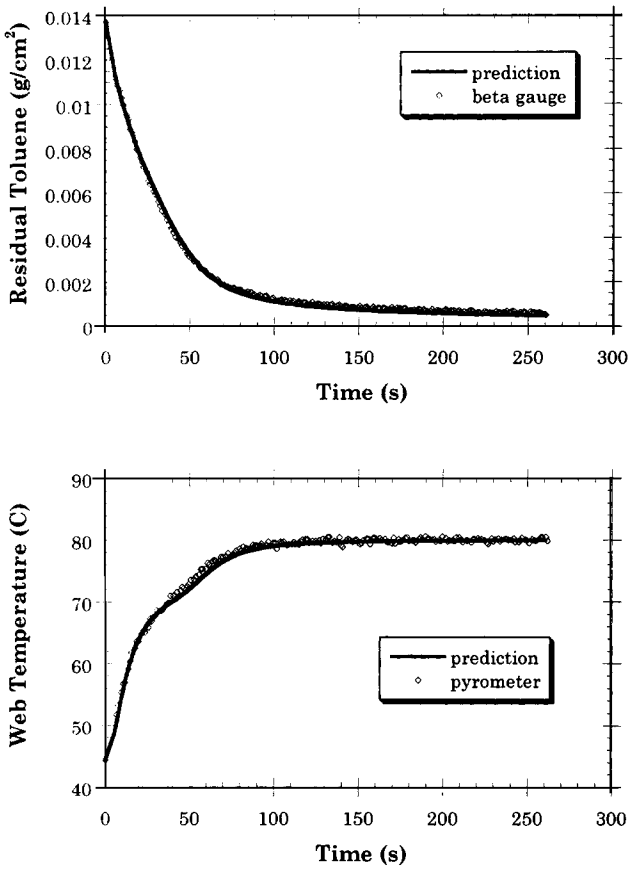

Figure 9. Measured and predicted residual solvent and web temperature profiles for a poly(vinyl acetate)/toluene coating on 3.56×10^{-3}-cm polyester in a parallel-flow pilot oven at 80°C.

The predictions are based on $h^g = h^G = 6.4\times10^{-4}$ cal/s·cm²·K, $\epsilon^S = \epsilon^P = 0.95$, and $\epsilon_l = \epsilon_u = 0.3$.

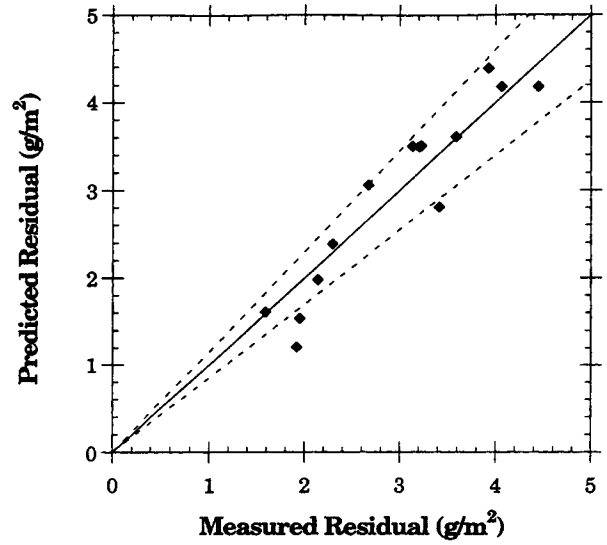

Figure 10. Predicted vs. measured residuals for natural rubber/heptane coatings on 3.56×10^{-3}-cm polyester in an air-floatation pilot oven at 80°C.

The predictions are based on $h^g = 2.1\times10^{-3}$ cal/s·cm²·K and $h^G = 2.5\times10^{-3}$ cal/s·cm²·K. The predictions do not include radiative heating. Dashed lines indicate 15% error bounds.

lation obtained from TEC Systems (De Pere, WI). This correlation gives an average heat-transfer coefficient based on the nozzle spacing, air flow rates, temperatures, and so forth. We did not explicitly account for the radiative heating in this case, but did use Eq. 20 to compute the coating-side mass-transfer coefficient. This clearly introduced some error into our predictions. Nonetheless, eleven out of the fourteen predictions are within 15% of the measured values.

Conclusions

Quantitative predictions of solvent drying rates from polymer/solvent coatings generally require an accurate description of the polymer/solvent mutual diffusion coefficients. Traditional techniques for characterizing mutual diffusion coefficients are difficult to implement for industrial coatings that may contain multiple polymers and/or other nonvolatile components and industrial-grade solvent(s). We have proposed a method for extracting *effective* free-volume parameters for the mutual diffusion coefficients in true or pseudobinary systems by using a detailed drying model and bench-top gravimetric experiments. The method shows excellent agreement with published data for poly(vinyl acetate)/toluene and yielded quantitatively accurate drying predictions for both poly(vinyl acetate)/toluene and a natural rubber-based adhesive in industrial-grade heptane. The method offers significant time savings in characterizing mutual diffusion coefficients and provides effective free-volume theory parameters for complex systems. We believe that such effective free-volume parameters will allow quantitatively accurate predictions of drying rates for a broad range of industrial coatings. The method may also find use in rapidly obtaining diffusion coefficients for application in other nondrying-related process calculations.

Acknowledgments

We gratefully acknowledge the commitment of Shuzo Fuchigami to fundamental process understanding and the open exchange of technical ideas. We also thank one of our reviewers for pointing out that radiative transport must be decoupled from the heat-transfer coefficient in order to apply the heat/mass-transfer analogy. This suggestion significantly improved the agreement of our model with pilot-scale experiments. Finally, we thank Walter Kerchee, Eric Grovender, and Andrew Metters for assisting with the pilot studies.

Literature Cited

Cairncross, R. A., "Solidification Phenomena during Drying of Sol-to-Gel Coatings," PhD Thesis, Univ. of Minnesota, Minneapolis (1994).

Cairncross, R. A., L. F. Francis, and L. E. Scriven, "Competing Drying and Reaction Mechanisms in the Formation of Sol-to-Gel Films, Fibers, and Spheres," *Drying Technol.*, **10**, 893 (1992).

Cairncross, R. A., S. Jeyadev, R. F. Dunham, K. Evans, L. F. Francis, and L. E. Scriven, "Modeling and Design of an Industrial Dryer with Convection and Radiant Heating," *J. Appl. Poly. Sci.*, **58**, 1279 (1995).

Dhatt, G., and G. Touzot, *The Finite Element Method Displayed*, Wiley, New York (1984).

Downham, R. E., J. F. Eckelaert, and J. W. Frost, "Floatation of Sheet Materials," U.S. Patent 3,549,070 (1970).

Duda, J. L., "Diffusion in Polymer Melts," *Devolatilization of Polymers*, Sect. III, J. A. Biesenberger, ed., Hanser, Munich (1983).
Garbow, B. S., K. E. Hillstrom, and J. J. More, *LMDIF1*, Argonne National Laboratory, Argonne, IL (1980).
Gutoff, E. B., "Modeling the Drying of Solvent Coatings on Continuous Webs," *J. Imaging Sci. Technol.*, **38**, 184 (1994).
Kreith, F., *Principles of Heat Transfer*, 3rd ed., Harper and Row, New York (1973).
Petzold, L. R., *DASSL*, Sandia National Laboratory, Livermore, CA (1983).
Robinson, D. E., A. E. Higinbotham, and P. C. Wankat, "Accelerated Polymer Film Drying at Elevated Pressures," *Ind. Eng. Chem. Process Des. Dev.*, **8**, 502 (1969).
Tu, Y., and R. L. Drake, "Heat and Mass Transfer during Evaporation in Coating Formation," *J. Colloid Interf. Sci.*, **135**, 562 (1990).
Vrentas, J. S., and J. L. Duda, "Diffusion in Polymer-Solvent Systems: I. Reexamination of the Free-Volume Theory," *J. Poly. Sci. Poly. Phys. Ed.*, **15**, 403 (1977a).
Vrentas, J. S., and J. L. Duda, "Diffusion in Polymer-Solvent Systems: II. A Predictive Theory for the Dependence of Diffusion Coefficients on Temperature, Concentration, and Molecular Weight," *J. Poly. Sci. Poly. Phys. Ed.*, **15**, 417 (1977b).
Vrentas, J. S., J. L. Duda, H. C. Ling, and A. C. Hou, "Free-volume Theories for Self-diffusion in Polymer-Solvent Systems: II. Predictive Capabilities," *J. Poly. Sci. Poly. Phys. Ed.*, **23**, 289 (1985).
Vrentas, J. S., and C. M. Vrentas, "Drying of Solvent-Coated Polymer Films," *J. Poly. Sci.: Part B: Polym. Phys.*, **32**, 187 (1994).
Zeilinski, J. M., and J. L. Duda, "Predicting Polymer/Solvent Diffusion Coefficients Using Free-Volume Theory," *AIChE J.*, **38**, 405 (1992).

Appendix

Assuming that no reactions occur in the coating and neglecting viscous dissipation, kinetic-energy effects, body-force effects, pressure work, and radiative heating, the energy balance for the polymer phase is

$$\frac{\partial}{\partial t}\sum_{i=1}^{2}\rho_i^P\hat{h}_i+\frac{\partial}{\partial x}\sum_{i=1}^{2}n_i^P\hat{h}_i=\frac{\partial}{\partial x}\left(\kappa^P\frac{\partial T^P}{\partial x}\right), \quad \text{(A1)}$$

where $\hat{h}_i$ is the specific enthalpy of each component, $\hat{h}_i = c_{p,i}(T^P - T_{\text{ref}})$ and n_i^P is the species flux in the polymer phase. The species continuity equation

$$\frac{\partial \rho_i^P}{\partial t}+\frac{\partial n_i^P}{\partial x}=0 \quad \text{(A2)}$$

allows us to reduce the energy balance to

$$\sum_{i=1}^{2}\rho_i^P c_{p,i}\frac{\partial T^P}{\partial t}+\sum_{i=1}^{2}n_i^P c_{p,i}\frac{\partial T^P}{\partial x}=\frac{\partial}{\partial x}\left(\kappa^P\frac{\partial T^P}{\partial x}\right). \quad \text{(A3)}$$

If we define the diffusive fluxes with respect to the volume-average velocity:

$$n_i^P=\rho_i^P v^{\ddagger}+j_i^P, \quad \text{(A4)}$$

note that the volume-average velocity is zero when there is no flux through the substrate (Vrentas and Vrentas, 1994), and use Fick's law

$$j_i^P=-D^P\frac{\partial \rho_i^P}{\partial x} \qquad \sum_{i=1}^{2}j_i^P\hat{V}_i=0, \quad \text{(A5)}$$

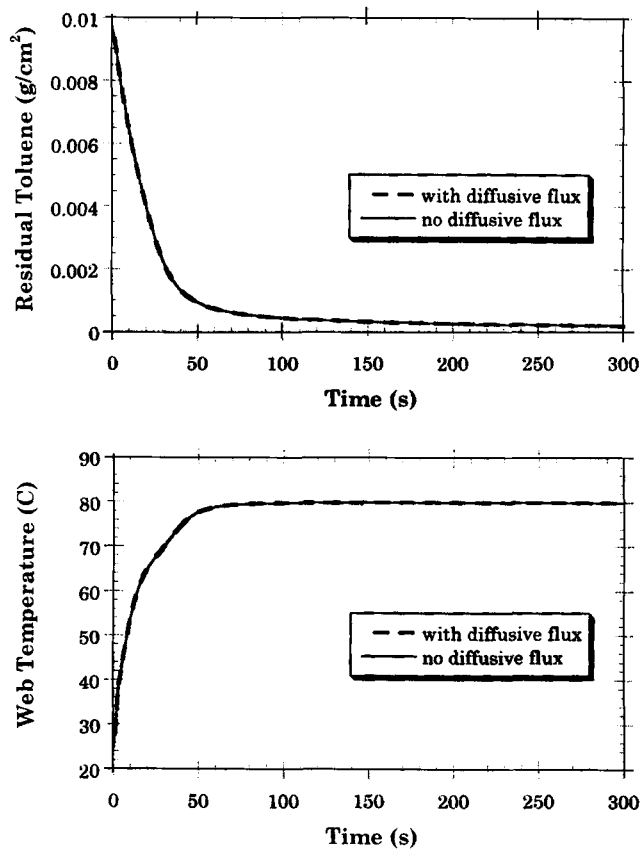

Figure A1. Residual solvent and average web temperature profiles for 4.19×10^{-3} g/cm² (dry wt.) of 30% solids poly(vinyl acetate) in toluene on 3.56×10^{-3}-cm polyester web with and without the interdiffusive flux in the energy balance (Eq. 15).

Neither calculation includes radiant heating. Materials parameters are shown in Table 1, except $c_{p,2}=1.0$. $h_l = h_a = 8.5\times10^{-4}$ cal/s·cm²·°C, and $T_{\text{oven}} = 80$°C.

then the energy balance reduces to

$$\rho^P c_p^P\frac{\partial T^P}{\partial t}=\frac{\partial}{\partial x}\left(\kappa^P\frac{\partial T^P}{\partial x}\right)+D^P\left(c_{p,1}-\frac{\hat{V}_1}{\hat{V}_2}c_{p,2}\right)\frac{\partial \rho_1^P}{\partial x}\frac{\partial T^P}{\partial x}. \quad \text{(A6)}$$

This is Eq. 15 in the text. The last term corresponds to the interdiffusive energy flux.

Figure A1 shows a test calculation for a case similar to that in Figure 9, using all of the parameters in Table 1 except $c_{p,2}=1.0$. The change in the polymer-specific heat for the test calculation exaggerates the effect of the interdiffusive energy flux. Figure A1 shows the predicted drying curves with and without the interdiffusive energy-flux term. The final solvent residuals, 1.94678×10^{-4} g/cm² with the flux term and 1.94684×10^{-4} g/cm² without the flux term, differ by much less than 1%. This small difference confirms our assumption that the interdiffusive energy flux can be neglected in typical calculations of the type described in this article.

Manuscript received Sept. 30, 1996, and revision received Mar. 21, 1997.